energies

MDPI

Article

Impact of Vibration on the Surface Film of Lithium-Ion Cells

Limhi Somerville [1], James Michael Hooper [1,*], James Marco [1], Andrew McGordon [1], Chris Lyness [2], Marc Walker [3] and Paul Jennings [1]

1 Warwick Manufacturing Group (WMG), University of Warwick, Coventry CV4 7AL, UK; l.somerville@warwick.ac.uk (L.S.); James.marco@warwick.ac.uk (J.M.); mcgord_a@wmg.warwick.ac.uk (A.M.); Paul.Jennings@warwick.ac.uk (P.J.)
2 Jaguar Land Rover, Banbury Road, Warwick CV35 0XJ, UK; clyness@jaguarlandrover.com
3 Department of Physics, University of Warwick, Coventry CV4 7AL, UK; m.walker@warwick.ac.uk
* Correspondence: j.m.hooper@warwick.ac.uk; Tel.: +44-(0)24-7657-3061

Academic Editor: K.T. Chau
Received: 24 March 2017; Accepted: 22 May 2017; Published: 25 May 2017

Abstract: Cylindrical 18650-type lithium-ion cells are being utilized more often for automotive applications. This introduces error in calculating expected lifetime due to varied usage conditions accelerating or reducing material damage. One such usage condition is vibration, which has been shown to impact the electrical performance over extended periods. Within this study X-ray photoelectron spectroscopy (XPS) has been performed on nickel manganese cobalt (NMC) cells subjected to vibration. This study found that vibration causes the removal of the selectively-formed surface film created during a cell's first cycles and replaces it with the surface film from electrolyte decomposition. The surface films formed by vibration are composed of much higher concentrations of organic electrolyte decomposition products than the film from the control cell. The impact of this chemical mechanism is an increased level of cell degradation. This is exhibited in increased capacity fade and cell impedance. This is the first study presented within the academic literature which has identified an electro-mechanical mechanism responsible for the performance degradation in lithium-ion cells from vibration.

Keywords: XPS; vibration; ageing; lifetime; cylindrical cells; vehicle use

1. Introduction

Legislative requirements are motivating vehicle manufacturers to integrate new powertrain technologies. Over the last few years, a number of hybrid and electric vehicles have been introduced alongside their traditional internal combustion engine counterparts. Rechargeable lithium-ion technology has been a key contributor to facilitating this [1,2]. Many manufacturers use cylindrical format cells (e.g., 18650) in their vehicles [3–6]. These cells are often chosen for economic reasons because they are a common form factor produced in large quantities and, thus, benefit from economies of scale and security of supply [6–8]. They are also chosen for safety reasons because of integrated features which prevent high current surges and gas build up [6–8], making the chance of explosion and fire less likely.

To ensure in-market reliability, vehicle manufacturers perform a variety of mechanical and durability tests during the design and prototype stages of the development process. These tests ensure that new vehicle components are fit-for-purpose and that they can meet the expected lifetime requirements. These tests also provide data to either parameterize or validate computer aided engineering (CAE) models and simulations. They also help to determine root cause of failure modes so that the robustness of the component can be improved. Vibration durability is one of

these tests and is performed to better understand the behavior of a given system when subjected to mechanically induced vibration that is representative of the in-service environment or desired vehicle life (typically 100,000 miles of customer usage). Vibration durability tests play an important role in the selection and lifetime prediction of components. As discussed within [9–13], vibration is a significant factor in the failure of automotive components due to mechanisms, such as fatigue cracking or the work-hardening of materials [11,14,15]. Within the context of Li-ion cells suitable for a contemporary EV battery application, a significant body of research exists that underpins the mechanical characterization of both pouch and cylindrical cell formats through quasi-static and dynamic test techniques. With respect to the quasi-static testing, there has been a clear focus on obtaining data from materials found within Li-ion cells through traditional mechanical assessment techniques, such as strain and bending [16–19], force displacement [16–20], and creep [19], as well as Li-ion cell-specific studies investigating tolerance changes during charge and discharge [21]. Within the dynamic testing domain there has been a significant focus towards assessing the crashworthiness and robustness of Li-ion cells via mechanical crush [16,20,22], penetration [18,23], impact resistance [16,22], and mechanical shock [16,24]. The research in the quasi-static and dynamic domains has been driven by a need to comply with whole vehicle crash homologation [25,26], to meet consumer focused accreditation requirements (e.g., Euro NCAP [27]) and mandatory transport legislation, such as UN 38.3 [28].

As discussed within [29], there has been very little research into how vibration impacts the internal components of lithium-ion cells and how the cells are aged at a microscopic level when subjected to a desired durability life. Brand et al. [24] performed vibration studies on 18650-type cylindrical cells and found that vibration caused short circuits from the mandrel moving up and down along the center of the cell; they showed images of where the mandrel created a hole through the center of the electrode tab. They also show what appears to be a melted separator, attributed to internal short circuits, and there is also some black soot deposit as well. However, their test was focused on providing energy along the mandrel axis and such forces, over long periods of time, are not likely to be exhibited over 100,000 miles. Svens [30] notes a potential mechanism for lithium iron phosphate cells which is more attributable to long-term effects of vibration aging. They found iron deposited at the negative electrode, presumably through fracture and subsequent dissolution at the positive electrode followed by migration to the negative electrode through the electrolyte. However, they provide no explanation of how samples were prepared for analysis and so the potential for contamination during cell opening and analysis is always a consideration in such cases.

This paper presents the results from a materials characterization study on four cells (numbered 3, 15, 17, and 18) from previous work on the impact of vibration to electrical performance [29]. The aim of the paper is to determine the internal mechanism(s) responsible for changes in the electrical performance of commercially-available 18650-type lithium-ion cells due to vibration.

2. Experimental Method and Theory

This study is an extension of that presented within [29] which identified that exposing commercially-available 18650-type nickel manganese cobalt (NMC) cells to vibration energy (representative of 100,000 miles North American customer usage) can result in increased levels of cell performance degradation through permanent capacity loss and an increase in the cell's internal impedance. While its effect on electrical performance was quantified through experimentation, the underlying causality was not defined in this previous work. It is beyond the scope of this study to define, in detail, the experimental method or the complete set of results obtained. However, to provide context for this research, pertinent elements are presented later.

2.1. Cells

This work used four commercially-available 2.2 Ah 18650-type cells comprised of a NMC positive electrode, graphite negative electrode with organic solvent; containing $LiPF_6$ salt. Three cells were

subjected to vibration in accordance with SAE J2380 [29], whilst the remaining sample was defined as a control cell. The control sample was not subject to any vibration. However, during vibration testing, the control sample was located in the same room and in close proximity to the other three test cells and therefore was subject to the same temperature and humidity.

2.2. Vibration and Electrical Characterization

Electrical characterization of the cells was conducted pre and post application of vibration so that a measurement of the changes in electrical performance could be determined. The electrical characterization methods employed to measure cell performance were:

- A 1 C capacity discharge (fully discharged at 1 C to 2.75 V)
- Pulse power testing (to determine DC resistance)
- Electrochemical impedance spectroscopy (EIS) (to determine ohmic and charge transfer resistance)
- Open cell voltage measurement (OCV)

Additional information and an in depth explanation on how these cells were vibrated and electrically-characterized is explained in [29]. Post application of vibration, all cells displayed performance degradation. The key specific changes with respect to Samples 3, 15, 17, and 18 are defined in Table 1. To ensure traceability with results mentioned in [29] the same cell sample numbers are used.

Table 1. Electrical performance change of four cells subjected to no vibration (control) and vibration (15, 17, and 18) taken from previous work by Hooper et al. [29]. The percentage values refer to the change from the cells' initial characterization.

Sample	1C Capacity (%)	DC Resistance (%)	OCV (%)	Ohmic Resistance (%)	Charge Transfer Resistance (%)
15	−1.83	92.4	0.03	254.5	24.1
17	−0.93	121.4	0.03	209.8	28.6
18	−6.76	79.5	0.05	203.7	35.2
3 (control)	0.00	1.0	0.2	1.4	32.3

2.3. Post-Test Analysis Cell Tear Down

Cells were opened, electrodes unwound, and samples prepared in an inert argon environment glove box with less than 1 ppm of both oxygen and water. The cells were opened using a method which did not produce sparks or contaminants from the cell can, or cut into the electrode jelly roll. The electrodes were stored separately in plastic bags. Cathode and anode samples were prepared for X-ray photoelectron spectroscopy (XPS) analysis separately and not in proximity to each other to limit cross-contamination. In addition, all samples were handled and cut with clean tweezers and scissors each time to further reduce the chance of sample cross-contamination. Three samples were taken from 10 mm in from along the length of the longest side of the unwound electrode from each cell and analyzed with XPS. After processing there was a total difference in relative area of the chemical environments of up to 5% between these samples, for this reason, differences of less than 5% will be deemed as insignificant.

2.4. XPS Analysis

Samples were transferred to the XPS system using an original manufacturer air-tight sample holder, shown in Figure 1. This transfer unit did not expose the sample to atmosphere at any stage. Samples were analyzed using a Kratos Axis Ultra DLD spectrometer (Kratos Analytical Ltd, Manchester, UK) with a base pressure of circa 2×10^{-10} mbar. XPS measurements were performed in the main analysis chamber, with the sample being illuminated using a monochromatic Al kα X-ray source. Measurements were conducted at room temperature and a take-off angle of 90° with respect to the surface parallel.

The core level spectra were recorded using a pass energy of 20 eV (resolution ca. 0.4 eV), from an analysis area of 300 µm × 700 µm. The spectrometer work function and binding energy scale were calibrated using the Fermi edge and 3d_5/2 peak recorded from a clean polycrystalline Ag sample prior to the commencement of the experiments. After acquisition, all spectra were referenced to the C 1s peak at 284.6 eV (before sputtering) and 284.4 eV (after sputtering). The data were processed using Shirley backgrounds and mixed Gaussian-Lorentzian (Voigt) line shapes. For compositional analysis, the analyzer transmission function has been determined using Ag, Au, and Cu foils to calibrate the detection efficiency across the full binding energy range. Sputtering was performed with an Ar^+ ion gun at 2 keV over an area of 3 × 3 mm. Samples were sputtered in 30 s periods until a steady state (the relative concentrations and peak positions does not change) was achieved in the material at which point no more sputtering occurred and the post-sputtered sample spectra was recorded. All negative electrode samples reached a steady state within one minute of sputtering.

Peak positions and chemical environments were established based on the fewest number of component parts for a fitting R^2 (a statistical measure of the variation that is explained by a linear model) of greater than 98% accuracy and in accordance with expected chemical environments for the system. Peak positions (binding energy) were maintained from sample to sample of less than 0.4 eV variance, and peak width (FWHM) had an identical restriction. The assignment of chemical environments is representative of expected binding energies, in accordance with established literature [29,31,32].

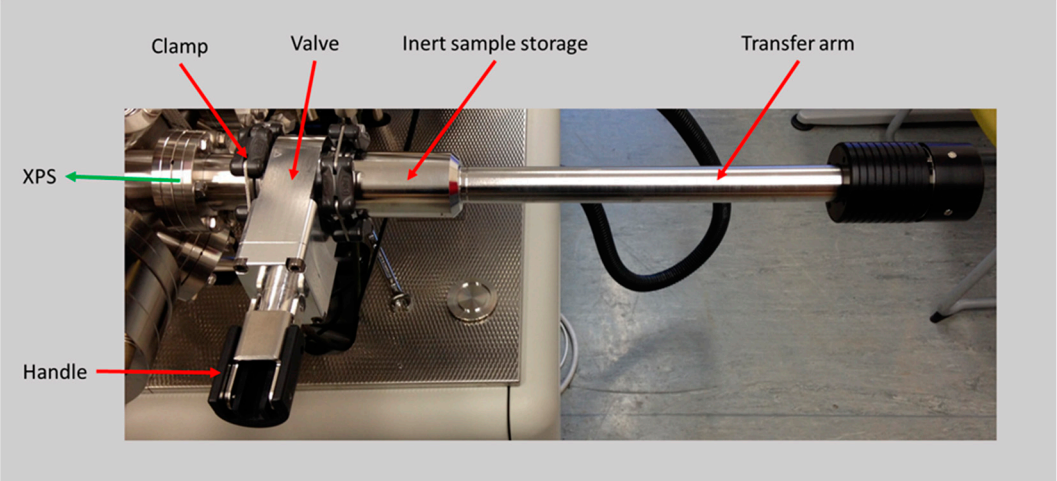

Figure 1. Kratos© XPS inert sample transfer chamber.

3. Results

3.1. Surface Film (Negative Electrode Post-Sputter)

Figure 2 contains C 1s XPS spectra of the negative electrode from the control cell and the three vibrated cells after sputtering and represents differences in the chemical composition of surface film between cells. There are three chemical environments which can be attributed to the spectra of the control cell; these are C–C from graphite (284.4 eV) [31–33] which will invariably include some C–H components that broaden the FWHM of the peak. A carbide, C–Li (282.8 eV), which is a component of the surface film [34] and also C–O (286.3 eV) which is a component of the surface film [31]. For each of the cells that have been vibrated, the authors identified an additional component within the surface film that is attributed to esters (O–C=O) (289 eV) [35]. On the basis that this component was not found in the control sample and yet is present in all of the vibrated cells, its presence has been asserted to a direct consequence of the cells being exposed to a vibration loading.

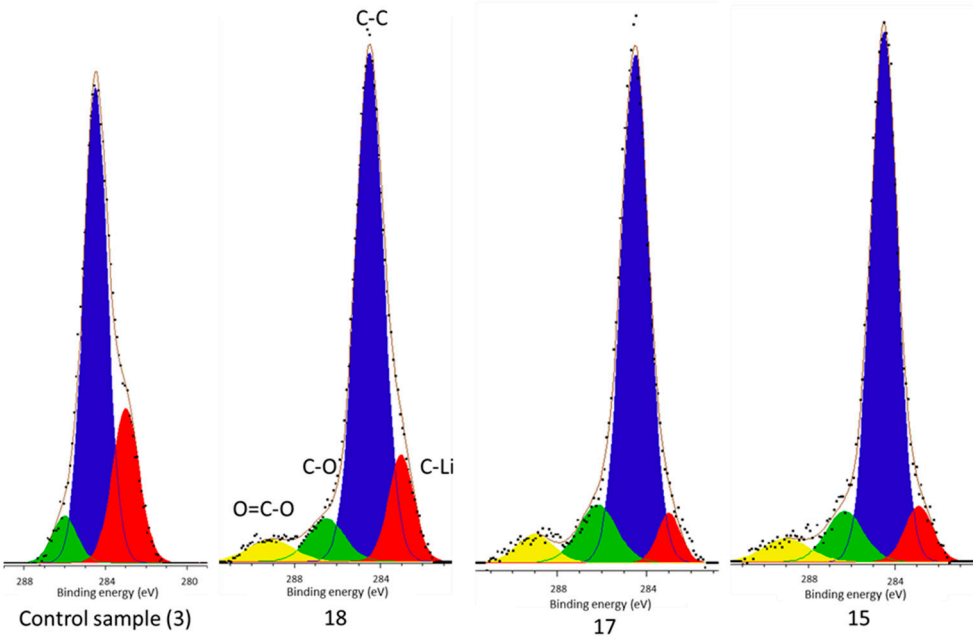

Figure 2. XPS spectra of the negative electrode for C 1s from four cells (3, 15, 17, and 18) after sputtering with Ar^+ ions. The chemical environments (C–Li etc.) are shown by tags in cell 18 and are identical in position and color to those shown in the other cells.

Figure 3 also supports the finding that there is no O–C=O in the control cell surface film. The O 1s spectra shows no evidence of the C=O environment at 533.6 eV for the control cell and, yet, it is present in each of the other cells which has been vibrated. The F 1s and P 2p spectra are included to show that there were no other significant changes in the chemical structure of the surface film with no evidence of additional bonding environments. The control, and cell 17's F 1s spectra, does contain a peak at 682.5 eV. This observation has been attributed to NaF contamination, which is consistent with the NIST XPS database allocation [36]. A noteworthy observation was the potential for Na to be present within the XPS spectra in these two cases. However the spectra was exceptionally noisy due to the very low concentrations present. In both cases the contribution from NaF is less than 1% of the total F environments and, thus, negligible.

All C environments in the C 1s spectra have been determined from the concentration of that peak relative to total carbon environments. However, the more reliable peak for species concentrations come from the P 2p spectra and the F 1s spectra because these are only present within the cell as $LiPF_6$ initially and, thus, any decomposition products containing either P or F must come from the same absolute concentration of $LiPF_6$.

Table 2 contains percentage concentrations of chemical environments detected from XPS. It shows an increase in the components corresponding to decomposition of the electrolyte in each of the vibrated cells. This is most notable for the phosphates which increased from 57% of P 2p environments to a minimum of 68% and a maximum of 73% in the vibrated cells. This represents the chemical degradation of $LiPF_6$ salt to form phosphates; it is most pronounced in vibrated cells. In addition, the absence of O–C=O containing compounds in the control sample yet presence, of up to 22% in the vibrated cells, shows that the chemical composition and not just the relative concentration of the surface film in the cells which were vibrated, has changed.

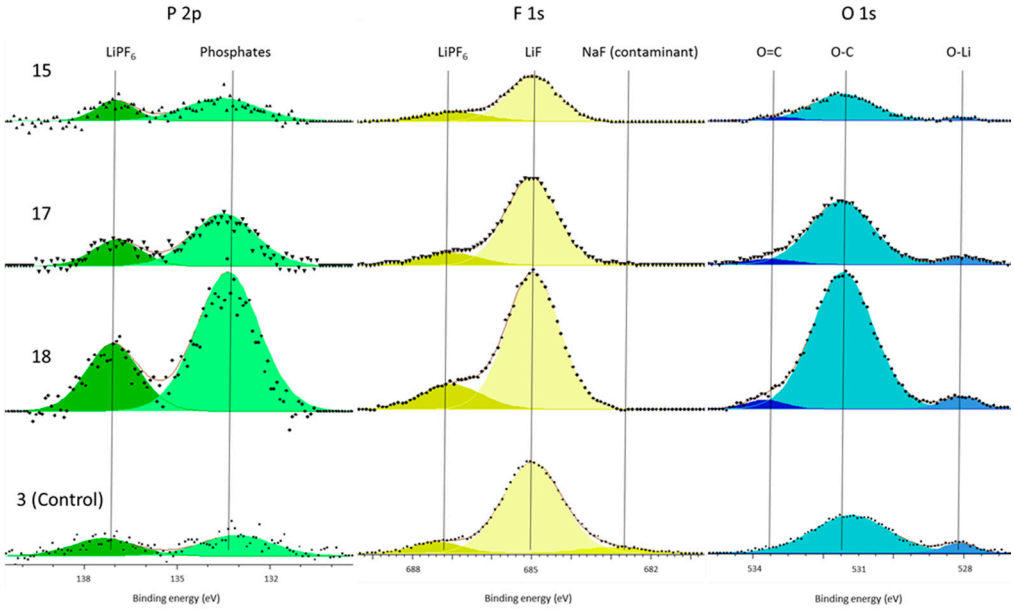

Figure 3. XPS spectra of the negative electrode for P 2p, F 1s, and O 1s from four cells (3, 15, 17, and 18) after sputtering with Ar^+ ions. The chemical environments are represented by tags (e.g., LiF) and lines which indicate the relative binding energy alignment.

Table 2. Relative percentages of chemical environments from chosen peaks and elemental environments in Figures 2 and 3.

Cell	LiF (F 1s)	C–O (C 1s)	O–C=O (C 1s)	Phosphates (P 2p)
3 (control)	12%	9%	0%	57%
15	21%	12%	20%	73%
17	14%	14%	6%	68%
18	17%	10%	22%	71%

3.2. Electrolyte Decomposition Products (Negative Electrode Pre-Sputter)

Figure 4 contains XPS spectra of the negative electrode from the control cell and the three vibrated cells before sputtering and represents changes in the electrolyte deposits. Attribution of chemical environment is identical to those shown in Figure 2. However, while the control sample contains C–C/C–H, C–O, and O=C–O environments, it does not contain a carbide peak (C–Li) at 282.8 eV. Given the absence of C–Li in the control sample, but with its presence in all vibrated cells it is clear that vibration is the cause.

Figure 5 contains XPS spectra from the P 2p, F 1s, and O 1s chemical environments of the electrodes pre-sputter. There are two key differences between the control cell and the cells which had been vibrated. First is that in each vibrated cell the percentage concentration from phosphates increases significantly when compared to the P 2p salt component. Secondly, there is an increase in total quantity of O–C chemical environments present in the vibrated cells compared to the control sample.

Table 3 contains percentage concentrations of different chemical environments from the electrolyte deposited products. Whilst the LiF concentration remains essentially identical (except for cell 17); the other three environments each show a significant increase in cells subjected to vibration. Comparing the vibrated cells to the control sample the phosphate component has increased by a factor of 2.5 to 5.5 in the vibrated cells, whilst the C=O component has increased by a factor of 2.25 to 6. The C–O component has also increased, by a factor of 1.4 to 2.2 in the vibrated cells.

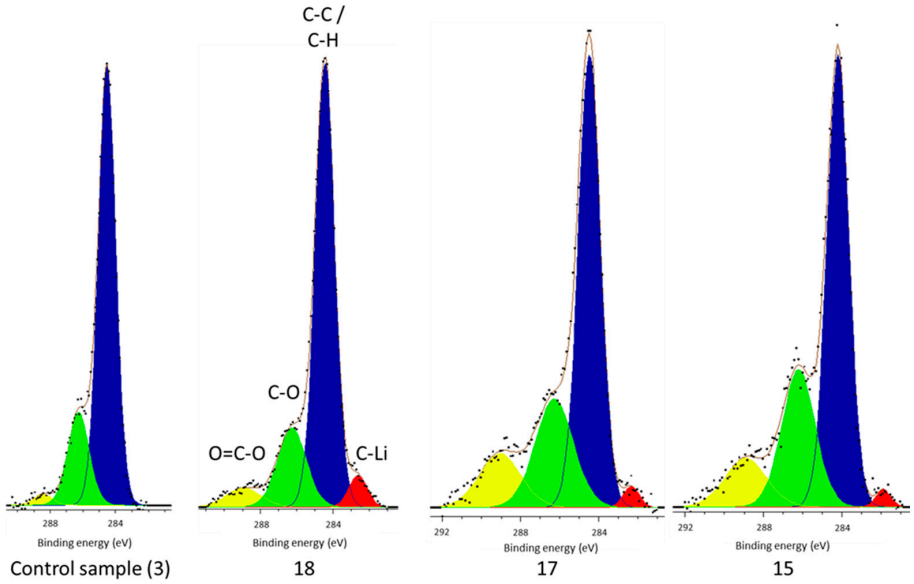

Figure 4. XPS spectra of the negative electrode for C 1s from four cells (3, 15, 17, and 18) before sputtering. The chemical environments (C–O etc.) are shown by tags in cell 18 and are identical to those shown in the other cells.

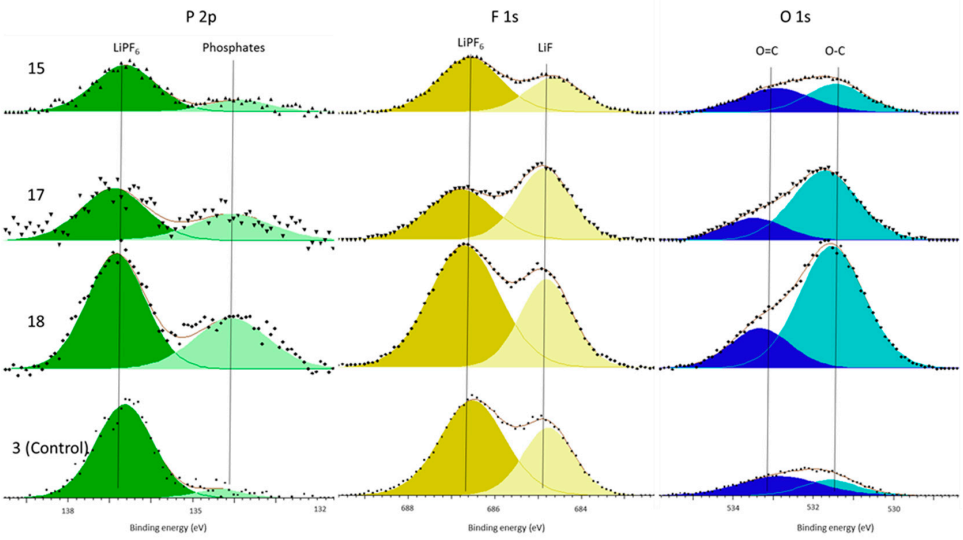

Figure 5. XPS spectra of the negative electrode for P 2p, F 1s, and O 1s from four cells (3, 15, 17, and 18) before sputtering. The chemical environments are represented by tags (e.g., LiF) and lines which indicate the relative binding energy alignment.

Table 3. Relative percentages of chemical environments from Figures 4 and 5.

Cell	LiF (F 1s)	C–O (C 1s)	O–C=O (C 1s)	Phosphates (P 2p)
3 (control)	36%	35%	3%	7%
15	35%	49%	18%	20%
17	53%	77%	19%	39%
18	35%	77%	7%	36%

Micrographs were collected with a scanning electron microscope (SEM) of both the positive and negative electrodes; however, there was no visual difference between the samples.

3.3. Positive Electrode

No differences between the control cell and vibrated cell positive electrode materials were observed. The peak positions and relative concentrations remained essentially identical throughout all of the cells and throughout sputtering.

4. Discussion

Part of the problem faced within the lithium-ion research community is the trade-off between understanding specific chemical mechanisms and obtaining answers which are accurate of in-use systems. This work has utilized commercially available 18650-type cells of unknown precise chemical composition. This was done to ensure that the results are representative of in-use conditions, however, since they are commercial cells it is not possible to know precisely which chemicals are present within the system and, therefore, precisely what reactants are present to form the surface film. This makes attributing a specific chemical mechanism for surface film formation complicated. However, it does mean that any conclusions reached are representative of real-world conditions and, therefore, directly relevant to industry practitioners and energy storage systems engineers tasked with designing and integrating complete battery assemblies for the automotive and road transport sector.

From this work it can be concluded that there is a carbide environment (C–Li) which comprises part of the surface film of each cell and the highest concentration is present in the control cell (Figure 2).

However, there is no carbide peak present in the electrolyte decomposition products of the control cell, but is present in each of the cells subject to vibration (Figure 4). It has been established that Li–C is a component of the surface film [34]. According to Aurbach its formation is dependent on a primary reaction of dimethyl carbonate (DMC) at the electrode surface with Li+ ions and electrons followed by a radical induced chain reaction with Li. They also suggest that this reaction probability is increased by the presence of a few ppm of H_2O in the electrolyte initially and, thus, would occur when the cell is manufactured [37] and not afterward. Its presence within the surface film decomposition products of only the vibrated cells yet in all cell surface films indicate that vibration is responsible. Since its formation happens shortly after manufacture vibration cannot be the source of the Li–C in the deposits, which is in accordance with the work of Aurbach et al., but rather liberated it from the surface film. Therefore, these results suggest that during vibration some of the surface film (including Li–C) breaks away from the electrode and is subsequently deposited within the cell electrolyte. The new film, which is indicated by the presence of O–C=O environments within the surface film of only vibrated cells, reforms in its place. As first presented in [38] and summarized in Table 1, the cell level manifestation of this reaction is a reduction in cell capacity and an increase in impedance.

In support of this principal mechanism the authors refer the reader to the presence of increased phosphate concentrations within the surface film and the electrolyte decomposition. The only source of phosphates is the $LiPF_6$ salt. This is known because there is no C–F component (binder) in the C 1s spectra (Figures 2 and 4) and because both the P 2p and F 1s (Figures 3 and 5) only have $LiPF_6$, as supported by the referenced literature. Therefore, the salt must have decomposed to form the additional phosphate components. Kawamura et al. show a possible mechanism for this phosphate formation in their work on the decomposition of $LiPF_6$ [39]. Although our work cannot definitively support this particular mechanism, it shows that salt decomposition occurs during cell formation and that this occurred more in the cells subjected to vibration.

In addition to lithium carbide in the electrolyte of vibrated cells and increased phosphate concentrations, the vibrated cells also contained higher concentrations of C–O and O–C=O environments in the electrolyte and increased LiF and C–O components in the surface film. It is well established that each of these components are part of the surface film, or products of its formation if found in the electrolyte, and that their increased concentration is suggestive of the increase in surface film forming reactions [31,32,35].

The presence of O–C=O environments within the vibrated cell surface film, with its absence in the control cell, further supports the previously-suggested mechanism. It would appear that vibration has

caused the removal of surface film from the electrode surface and then new surface film took its place, because the conditions are now different (i.e., lower concentrations of H_2O), the chemical composition of the surface film is different, hence the inclusion of O–C=O components. Etacheri et al. showed that the main reduction products for ethylene carbonate, propylene carbonate, and DMC contain ester compounds (O–C=O) [40]. It is also documented that commercial cells use additives such as vinylene carbonate to selectively react at the surface of electrodes initially [41] as sacrificial reactions to that of organic electrolyte solvents. They use specific quantities of these additives to form a surface film which uses up as little of the useful electrolyte components as possible without impeding cell function later [42]. Therefore, no matter the precise composition of the electrolyte used in these commercial cells, initially the product (new surface film formed after vibration) is likely to lead to an increased concentration of ester environments, causing an increased impedance and increased cell resistance as the surface film is no longer selectively formed for its role. The replacement of the selectively-formed film, that is purpose-built for its role, with a film that is the product of normal electrolyte reduction is the cause of cell aging for vibrated cells. It may be possible to mitigate the effect of aging if higher concentrations of the selective additives for improving cell surface film performance were included during cell manufacture.

The cells subjected to vibration all exhibited increased DC resistance and reduced capacity, which is consistent with the increased surface film. The formation of surface film and its composition has been shown to increase cell resistance [29]. The sharp increase in ohmic resistance of the vibrated cells can be attributed to either intercalation at the electrode surface, caused by a more ionically-resistant surface film, or an increase in electrolyte resistance. Both of these are exhibited in the XPS results (see Figure 2) by the presence of O–C=O components after vibration, which are known to be ionically resistant, which would potentially increase both DC and ohmic resistance. In addition, higher concentrations of C–O, O–C=O, and phosphate components were found in the electrolyte deposits. Since these products are formed from electrolyte, their presence indicates not only that transfer through the electrolyte is more difficult, but also that the cell contains less electrolyte solvent after vibration. Since these cells are commercial, no specific mechanism has been suggested for the capacity loss, itself, however, it is well established that lithium is consumed by the reaction at the exposed electrode surface [35]. Therefore, the mechanism suggested in our work is similarly consistent with a reduction in capacity. Vibration is reducing the cell performance in a similar manner to that of cycling cells, by removal, and then replacement, of the surface film.

It is recommended that original equipment manufacturers that use or make lithium-ion cells use a vibration profile within their testing procedures to determine expected cell lifetime.

5. Further Work

Having established these results, the authors would add that quantitative analysis of peaks for lithium-ion cells is difficult with XPS due to the number and variety of chemical species present in commercial cells and different vibration conditions; coupled with different chemical environments which can have similar binding energy. In addition, there are multiple different interpretations of the data and, as such, conclusions have only been made where the change in relative percentages of peaks is significant (>5%) and, thus, not open to variances in the C–C/C–H dependencies, or inadvertent bias introduced through peak selection. In essence, the authors have been careful to not over-interpret small changes in chemical composition between cells and made sure that only significant differences are considered. The XPS data fitting used is consistent for most of the chemical environments studied, however, there are variances in the percentage values of some C–O and O–C=O components between vibrated cells, as shown in Figure 4 and recorded in Table 3. The difference in these values may relate to the inherent differences in cell performance between identical cell types, as shown in [38].

Over the course of this test, the cells were subject to a representative 10 years of vehicle vibration and very few other variations in conditions. During 10 years of actual use, the cell will be subjected to many other competing factors, such as temperature, state of charge, and other storage or cycling

conditions. Vibration may play a minor part compared to these factors over a whole vehicle lifetime. However, its ability to remove surface film that has been selectively formed for its passivating abilities is unique from other mechanisms that temperature or state of charge induce and, therefore, may play a significant part in cell performance decline, especially when coupled with these other conditions.

The experimental results presented within [29], highlight the potential dependency between the charge state of the cells and the level of vibration induced degradation. Within this paper, the primary objective was to ascertain and to quantify the underpinning causes of the capacity loss and the impedance rise reported within [29]. This was achieved using a subset of the cell samples from [29]. One area of future research would be to extend these results through a more comprehensive evaluation program in which multiple cells conditioned to different SOC levels are subject to vibration energy before undertaking XPS analysis. The aim of this further work would be to better understand if the degradation modes identified within this initial study are realized across the complete SOC range that the cells may be expected to operate within for a typical EV application.

It is acknowledged the limited dataset employed, in terms of cells initially exposed to vibration loading and the subset studied through post-mortem analysis. Whilst the authors are confident that the results presented here highlight the underlying causality between cell vibration and performance degradation, it is believe that these initial results warrant further research. Especially because the concentration of some chemical environments (C–O/O–C=O), presented in Table 3, consistently vary between cells and, therefore, the type of vibration may induce a change in the surface film formed. It is, therefore, recommended that the scope of the experimental study to encompass cells from a broader cross-section of manufacturers, form-factors, and chemistries be expanded. This will identify if the experimental results presented here are transferable to other cell technologies. In addition, the mechanism of film formation proposed here requires further study and this would be improved by including additional analytical techniques to further elucidate the surface film composition of the replacement film that forms.

6. Conclusions

Electrical data had previously shown that vibration causes capacity and power loss in lithium-ion cells. On closer inspection there is evidence that this is caused by removal of a selectively-formed surface film and replacement with a surface film formed from electrolyte decomposition. Vibration caused the electrode surface film to break off. This conclusion is based on the presence of lithium carbide in the electrolyte-deposited products of vibrated cells and yet not in the control cell. This is further supported by increases in the percentage of C–O, C=O (O 1s) and phosphates (P 2p) in the electrolyte deposits, which were caused in the production of surface film. In addition, the presence of ester compounds (O–C=O) in the vibrated cell's surface film and absence in the film of the control cell suggests that the formation of the surface film is a secondary reaction and not formed until after the C–Li and other primary surface films have vibrated off of the active material surface. Since this is a different mechanism to those induced through temperature or state of charge; vibration testing may need to be considered for lifetime prediction of lithium-ion cells for automotive use.

Acknowledgments: This research was supported by the Engineering and Physical Science Research Council (EPSRC—EP/I01585X/1). The research was undertaken in collaboration with the WMG center High Value Manufacturing Catapult (funded by Innovate UK) and Jaguar Land Rover.

Author Contributions: Limhi Somerville conceived and designed the experiments; Limhi Somerville performed the experiments; Limhi Somerville, James Michael Hooper, and Marc Walker analyzed the data; James Michael Hooper and Chris Lyness contributed test samples and data from vibration durability study; James Marco, Andrew McGordon, Marc Walker, Chris Lyness, and Paul Jennings provided academic research supervision; Limhi Somerville and James Michael Hooper wrote the paper; and James Marco, Andrew McGordon, Marc Walker, Chris Lyness, and Paul Jennings provided peer review of paper.

Conflicts of Interest: The authors declare no conflict of interest.

References

1. Jackson, N. Technology road map, r+d agenda and UK capabilities. In *Cenex Low Carbon Vehicle Show 2010*; Automotive Council UK: London, UK; Millbrook Proving Ground: Bedfordshire, UK, 2010; pp. 1–16.
2. Parry-Jones, R. *Driving Success—A Strategy for Growth and Sustainability in the UK Automotive Sector*; Automotive Council UK: London, UK, 2013; pp. 1–87.
3. Day, J. Johnson Controls' Lithium-Ion Batteries Power Jaguar Land Rover's 2014 Hybrid Range Rover. Available online: http://johndayautomotivelectronics.com/johnson-controls-lithium-ion-batteries-power-2014-hybrid-range-rover/ (accessed on 17 February 2015).
4. Rawlinson, P.D. Integration System for a Vehicle Battery Pack. U.S. Patent 20120160583 A1, 28 June 2012.
5. Berdichevsky, G.; Kelty, K.; Straubel, J.; Toomre, E. *The Tesla Roadster Battery System*; Tesla Motors: Palo Alto, CA, USA, 2007; pp. 1–5.
6. Kelty, K. *Tesla—The Battery Technology behind the Wheel*; Tesla Motors: Palo Alto, CA, USA, 2008; pp. 1–41.
7. Paterson, A. *Our Guide to Batteries*; Axeon: Aberdeen, UK, 2012; pp. 1–22.
8. Anderman, M. The tesla battery report. In *Tesla Motors: Battery Technology, Analysis of the Gigafactory, and the Automakers' Perspectives*; Advanced Automotive Batteries: Oregon House, CA, USA, 2014; pp. 1–39.
9. Karbassian, A.; Bonathan, D.P. Accelerated vibration durability testing of a pickup truck rear bed. *SAE Int.* **2009**, 1–5. [CrossRef]
10. Risam, G.S.; Balakrishnan, S.; Patil, M.G.; Kharul, R.; Antonio, S. Methodology for accelerated vibration durability test on electrodynamic shaker. *SAE Int.* **2006**, *1*, 1–9.
11. Harrison, T. *An Introduction to Vibration Testing*; Bruel and Kjaer Sound and Vibration Measurement: Naerum, Denmark, 2014; p. 11.
12. Hooper, J.; Marco, J. Experimental modal analysis of lithium-ion pouch cells. *J. Power Sources* **2015**, *285*, 247–259. [CrossRef]
13. Moon, S.-I.; Cho, I.-J.; Yoon, D. Fatigue life evaluation of mechanical components using vibration fatigue analysis technique. *J. Mech. Sci. Technol.* **2011**, *25*, 611–637. [CrossRef]
14. Halfpenny, A.; Hayes, D. *Fatigue Analysis of Seam Welded Structures Using Ncode Designlife*; HBM nCode: Rotherham, UK, 2013; pp. 1–21.
15. Halfpenny, A. Methods for accelerating dynamic durability tests. In Proceedings of the 9th International Conference on Recent Advances in Structural Dynamics, Southampton, UK, 17–19 July 2006; University of Southampton: Southamption, UK, 2006.; pp. 1–19.
16. Avdeev, I.; Gilaki, M. Structural analysis and experimental characterization of cylindrical lithium-ion battery cells subject to lateral impact. *J. Power Sources* **2014**, *271*, 382–391. [CrossRef]
17. Zhang, X.; Wierzbicki, T. Characterization of plasticity and fracture of shell casing of lithium-ion cylindrical battery. *J. Power Sources* **2015**, *280*, 4–56. [CrossRef]
18. Choi, H.Y.; Lee, J.S.; Kim, Y.M.; Kim, H. *A Study on Mechanical Characteristics of Lithium-Polymer Pouch Cell Battery for Electrci Vehicle*; 13-0115; Hongik University: Seoul, Korea, 2013; pp. 1–10.
19. Berla, L.; Lee, S.W.; Cui, Y.; Nix, W. Mechanical behavior of electrochemically lithiated silicon. *J. Power Sources* **2015**, *273*, 41–51. [CrossRef]
20. Greve, L.; Fehrenbach, C. Mechanical testing and macro-mechanical finite element simulation of the deformation, fracture, and short circuit initiation of cylindrical lithium ion battery cells. *J. Power Sources* **2012**, *214*, 377–385. [CrossRef]
21. Oh, K.-Y.; Siegel, J.; Secondo, L.; Kim, S.U.; Samad, N.; Qin, J.; Anderson, D.; Garikipati, K.; Knobloch, A.; Epureanu, B.; et al. Rate dependence of swelling in lithium-ion cells. *J. Power Sources* **2014**, *267*, 197–202. [CrossRef]
22. Sahraei, E.; Meiera, J.; Wierzbicki, T. Characterizing and modeling mechanical properties and onset of short circuit for three types of lithium-ion pouch cells. *J. Power Sources* **2014**, *247*, 503–516. [CrossRef]
23. Feng, X.; Sun, J.; Ouyang, M.; Wang, F.; He, X.; Lu, L.; Peng, H. Characterization of penetration induced thermal runaway propagation process within a large format lithium ion battery module. *J. Power Sources* **2015**, *275*, 261–273. [CrossRef]
24. Brand, M.J.; Schuster, S.F.; Bach, T.; Fleder, E.; Stelz, M.; Gläser, S.; Müller, J.; Sextl, G.; Jossen, A. Effects of vibrations and shocks on lithium-ion cells. *J. Power Sources* **2015**, *288*, 62–69. [CrossRef]

25. United Nations. *Ece r100—Battery Electric Vehicles with Regard to Specific Requirements for the Construction, Functional Safety and Hydrogen*; United Nations: New York, NY, USA, 2002.
26. Economic Commission for Europe (ECE). *Proposal for the 02 Series of Amendments to Regulation no. 100 (Battery Electric Vehicle Safety)*; Economic and Social Council ECE/TRANS/WP.29/2012/102; ECE: Geneva, Switzerland, 2013; pp. 1–54.
27. The Tests Explained. Available online: http://www.euroncap.com/testprocedures.aspx (accessed on 9 February 2015).
28. United Nations. *Transport of Dangerous Goods—Manual of Tests and Criteria—Fifth Edition—Amendment 1*; United Nations: New York, NY, USA, 2011; p. 62.
29. Hooper, J.M.; Marco, J.; Chouchelamane, G.H.; Lyness, C. Vibration durability testing of nickel manganese cobalt oxide (NMC) lithium-ion 18,650 battery cells. *Energies* **2016**, *9*, 52. [CrossRef]
30. Svens, P. Methods for Testing and Analyzing Lithium-Ion Battery Cells Intended for Heavy-Duty Hybrid Electric Vehicles. Ph.D. Thesis, KTH Royal Institute of Technology, Stockholm, Sweden, 2014.
31. Dedryvère, R.; Laruelle, S.; Grugeon, S.; Gireaud, L.; Tarascon, J.-M.; Gonbeau, D. XPS identification of the organic and inorganic components of the electrode/electrolyte interface formed on a metallic cathode. *J. Electrochem. Soc.* **2005**, *152*, A689–A696. [CrossRef]
32. Leroy, S.; Blanchard, F.; Dedryvere, R.; Martinez, H.; Carre, B.; Lemordant, D.; Gonbeau, D. Surface film formation on a graphite electrode in li-ion batteries: AFM and XPS study. *Surf. Interface Anal.* **2005**, *37*, 773–781. [CrossRef]
33. Blyth, R.; Buqa, H.; Netzer, F.; Ramsey, M.; Besenhard, J.; Golob, P.; Winter, M. XPS studies of graphite electrode materials for lithium ion batteries. *Appl. Surf. Sci.* **2000**, *167*, 99–106. [CrossRef]
34. Hu, Y.; Kong, W.; Li, H.; Huang, X.; Chen, L. Experimental and theoretical studies on reduction mechanism of vinyl ethylene carbonate on graphite anode for lithium ion batteries. *Electrochem. Commun.* **2004**, *6*, 126–131. [CrossRef]
35. Aurbach, D.; Markovsky, B.; Weissman, I.; Levi, E.; Ein-Eli, Y. On the correlation between surface chemistry and performance of graphite negative electrodes for li ion batteries. *Electrochim. Acta* **1999**, *45*, 67–86. [CrossRef]
36. *NIST Standard Reference Database 20*, version 4.1; National Institute of Standards and Technology: Gaithersburg, MD, USA, 2003.
37. Aurbach, D. Review of selected electrode–solution interactions which determine the performance of li and li ion batteries. *J. Power Sources* **2000**, *89*, 206–218. [CrossRef]
38. Kawamura, T.; Okada, S.; Yamaki, J.-I. Decomposition reaction of LiPF 6-based electrolytes for lithium ion cells. *J. Power Sources* **2006**, *156*, 547–554. [CrossRef]
39. Etacheri, V.; Marom, R.; Elazari, R.; Salitra, G.; Aurbach, D. Challenges in the development of advanced Li-ion batteries: A review. *Energy Environ. Sci.* **2011**, *4*, 3243–3262. [CrossRef]
40. Sato, T.; Maruo, T.; Marukane, S.; Takagi, K. Ionic liquids containing carbonate solvent as electrolytes for lithium ion cells. *J. Power Sources* **2004**, *138*, 253–261. [CrossRef]
41. Burns, J.; Petibon, R.; Nelson, K.; Sinha, N.; Kassam, A.; Way, B.; Dahn, J. Studies of the effect of varying vinylene carbonate (vc) content in lithium ion cells on cycling performance and cell impedance. *J. Electrochem. Soc.* **2013**, *160*, A1668–A1674. [CrossRef]
42. Aurbach, D.; Markovsky, B.; Shechter, A.; Ein-Eli, Y.; Cohen, H. A comparative study of synthetic graphite and Li electrodes in electrolyte solutions based on ethylene carbonate-dimethyl carbonate mixtures. *J. Electrochem. Soc.* **1996**, *143*, 3809–3820. [CrossRef]